Korean J. Chem. Eng., 36(12), 2095-2103 (2019)
DOI: 10.1007/s11814-019-0415-7

pISSN: 0256-1115
eISSN: 1975-7220

Modified kinetic rate equation model for cooling crystallization

Yuntae Jin*,‡, Kiho Park,‡, and Dae Ryook Yang*,†**

*Department of Chemical and Biological Engineering, Korea University, Seoul 02851, Korea
**School of Civil, Environmental and Architectural Engineering, Korea University, Seoul 02851, Korea
(*Received 21 May 2019 • accepted 25 October 2019*)

Abstract−The kinetic rate equation (KRE) model, unlike the population balance equation model, can describe growth, nucleation, and even Ostwald ripening simultaneously. However, the KRE model cannot be applied in cooling crystallization systems. In this work, we propose a modified KRE model to describe cooling crystallization. The modified KRE model can successfully describe crystal growth and nucleation in cooling crystallization systems. In addition, the metastable zone width was simulated using the modified KRE model and compared with the experimental data in references. The results revealed that the modified KRE model could express the effect of overheating prior to cooling on the metastable zone width. As the extent of overheating increases, the metastable zone width becomes wider, which phenomenon can be clearly simulated by the modified KRE model. This modeling capability is attributed to the behavior of particle clusters that are sized less than the size of sub-nuclei. Because the population balance equation model cannot describe the metastable zone width, the modified KRE model has certain competitive advantages in its application to various crystallization systems.

Keywords: Modeling, Crystallization, Population Balance, Metastable Zone Width, Cooling Crystallization

INTRODUCTION

Crystallization has been utilized to separate the solute from the solvent. Beginning with sodium chloride production, it has been used in various industries including pharmaceutical, petroleum, and fine chemicals [1-6]. To provide a theoretical background, multiple attempts have been made to describe crystallization using a mathematical model [7-16].

The population balance model is one of the most widely and frequently used models in both academic and industrial fields [17-24]. Proposed by Hulburt and Randolph as early as 1960s, the popularity of the model has increased steadily [17,25,26]. The applications of the population balance model are not limited to chemical engineering, but extend to astrophysics, biology, telecommunication, and transportation [17]. However, the population balance model lacks in the description of particle clusters smaller than the nucleus, as it is assumed that particles move from their suspended liquid form into a nucleus form at a certain degree of supersaturation [27-29].

To overcome such limitations, a master equation model had been proposed which accounts for the movements due to the attachment and detachment of individual particle clusters [30]. The kinetic treatment of nucleation in terms of the cluster approach was initiated by Szilard and Farkas [31], and further developed by Kaischew, Stranski, Becker, Doring, and Zeldovich [32,33]. Beginning with monomers, the master equation model counted the numbers of particle clusters at each size and expressed growth and dissolution in terms of attachment and detachment of the particle clusters, respectively. However, the population balance equation model describes nucleation as a boundary condition of the differential equations. Nucleation size is determined arbitrarily, as there is no descriptive equation for particle clusters smaller than the predetermined nuclei. Therefore, unlike the population balance model, the master equation model can describe particle clusters that are smaller than crystal nuclei.

The description of sub-nucleus sized clusters can lead to further investigations of the effect of pre-history on the temperature profile. Even though two solutions with same temperature are cooled for crystallization, the crystal size distributions from the two solutions can be different due to the difference of pre-history on the temperature profile. Multiple studies have shown that the prehistory associated with the temperature profile affects the induction time [34-36]. Further dissolution of subnucleus sized particle clusters subjected to overheated pre-history temperatures may explain the extended induction time. However, the dissolution of sub-nucleus sized particle clusters is not expressible by the population balance model. Therefore, the master equation model is required.

Despite these advantages of the master equation model, it has not been used widely enough to reflect its potential because of the large number of calculations required to apply it. Recently, a novel approach to the obstacle was suggested by Vetter et al. [27]. Named the kinetic rate equation (KRE) model, the model was simplified by utilizing the Cooper-Chang algorithm and making several assumptions.

While the development of the KRE model can extend the applicability of the master equation model to crystallization processes, one of its assumptions imposes a limitation on the utilization of the KRE model in an actual industrial process [37,38]. The KRE model developed by Vetter et al. assumes that the system was under an isothermal condition, and supersaturation was assumed as an initial condition [27]. Such an assumption in actual industry would indi-

†To whom correspondence should be addressed.
E-mail: dryang@korea.ac.kr
‡The authors equally contributed to this work.

cate a large instantaneous decrease in temperature. In reality, such decreases in temperature are never experienced; therefore, the model should be modified to reflect the occurrence of supersaturation caused by a temperature decrease to describe the actual crystallization processes.

In this study, we propose a modified version of the KRE model to improve the applicability of the KRE model for the cooling crystallization system. The modified KRE model accounts for the occurrence of supersaturation through a gradual temperature decrease. Simultaneously, the model describes the formation of crystals and their growth. Fully extended, the model may estimate resulting crystal distribution and induction time from cooling crystallization under various temperature profiles. The model was validated by comparing the final crystal distribution and induction time resulting from its application with those of experiments from previous literatures. From this study, the applicability of the KRE model can be extended to the cooling crystallization system, and the potential of the KRE model can be widely utilized in various crystallization systems.

DEVELOPING THE KRE MODEL

The KRE model classifies particle behavior into two groups: attachment and detachment. Every type of crystal growth and dissolution can be expressed by the following pseudo-equation:

$$P_n + P_m \underset{h_{n+m,n}}{\overset{g_{n,m}}{\rightleftarrows}} P_{n+m}, \tag{1}$$

where P_n stands for the number of particles consisting of n molecules, and $g_{n,m}$ and $h_{n+m,n}$ denote the attachment (n molecules and m molecules are attached to become n+m molecules) and detachment (n+m molecules are split into n molecules and m molecules) rates of particles, respectively. Utilizing the pseudo-equation above, four main particle behaviors in crystallization can be expressed: growth, agglomeration, dissolution, and breakage. The attachment rate $g_{n,m}$ can be accounted for by growth and agglomeration, while the detachment rate $h_{n+m,n}$ can be accounted for by dissolution and breakage. Following Kashchiev's work, the attachment rate and detachment rate can be expressed as [30]:

$$g_n = k \cdot n^a \tag{2}$$

$$h_n = k \cdot n^a \cdot P_1^*(n), \tag{3}$$

where k and a are the kinetic parameters dependent on each material. In this study, the values $k=6.86\times10^{-18}$ (m^3/s) and a=1/3 by Kashchiev were used [30]. $P_1^*(n)$ denotes the solubility of n-sized crystal.

This indicates that every particle behavior can be expressed in a single, continuous model, which may prove helpful in crystallization studies regarding agglomeration and breakage. However, the purpose of this study was to modify the KRE model for describing nucleation and growth under non-isothermal conditions. Therefore, agglomeration and breakage have not been considered in this model for the sake of simplicity.

As mentioned in the introduction, the population balance equation model expresses nucleation through a boundary condition. Therefore, the subnuclei-sized particle clusters cannot be described in the population balance equation model. In addition, crystallization behavior in the metastable zone width should be described with a factitious structure in the nucleation rate equation. However, the KRE model can describe the subnuclei-sized particle behavior clearly. The KRE model is based on molecular interaction, hence the crystallization characteristics such as a metastable zone and the induction time described by the KRE model have a strong theoretical background. Thus, modeling them by the KRE model does not need support from an artificial structure in the model equations. Despite these advantages, the KRE model is very complex and requires burdensome calculations. Thus, the simplification of the KRE model is very important before it can be applied successfully.

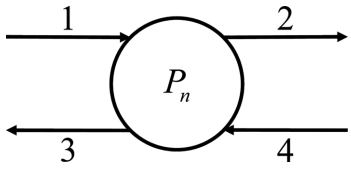

Fig. 1. Schematic diagram of KRE model. Each arrow represents attachments and detachments of particle clusters.

1. Simplification of the KRE Model

From Eq. (1), the change in the number of n-sized particles (P_n) in time can be described by the Fig. 1.

Particle attachment and detachment can now be expressed by the following ordinary differential equation:

$$\frac{dP_1}{dt} = 2 \cdot h_2 \cdot P_2 + \sum_{n=3}^{\infty} h_n \cdot P_n - 2 \cdot g_1 \cdot P_1^2 - P_1 \cdot \sum_{m=2}^{\infty} g_m \cdot P_m \tag{4}$$

$$\frac{dP_n}{dt} = \underbrace{\sum_{a=1}^{n-1} g_{a,\,n-a} \cdot P_a \cdot P_{n-a}}_{1} - \underbrace{\sum_{b=1}^{\infty} g_{b,\,n} \cdot P_n \cdot P_b}_{2} - \underbrace{\sum_{c=1}^{n-1} h_{n,\,c} \cdot P_n}_{3} + \underbrace{\sum_{d=n+1}^{\infty} h_{d,\,n} \cdot P_d}_{4} \tag{5}$$

for n≥2

where every possible attachment and detachment combination is included in the system. Each term on the right-hand side in Eq. (5) describes molecular movements, which are arranged in numerical order in Fig. 1.

However, to decrease the calculation complexity of the model, Vetter et al. considered only monomer attachment and detachment [27]. Therefore, Eq. (5) can be changed into the following form:

$$\frac{dP_n}{dt} = g_{n-1} \cdot P_1 \cdot P_{n-1} + h_{n+1} \cdot P_{n+1} - g_n \cdot P_1 \cdot P_n - h_n \cdot P_n \tag{6}$$

Even with the assumption that only monomers undergo attachment and detachment, the set of ordinary differential equations still has a large calculation complexity. Vetter et al. further simplified the model by transforming the model into a continuous form by utilizing Kashchiev's work [27,30]. The resulting Fokker-Planck equation is:

$$\frac{\partial \tilde{P}}{\partial t} + \frac{\partial}{\partial \tilde{n}}\left[v \cdot \tilde{P} - \frac{1}{2} \cdot \frac{\partial (H \cdot \tilde{P})}{\partial \tilde{n}} \right] = 0 \tag{7}$$

In Eq. (7), discrete particle size n and the number of particles P are

replaced by their counterparts ñ and $\tilde{P}$. Newly added variable v and H represent the growth rate and effective dispersion, respectively.

The transformation from the discrete model to the continuous model resulted in a model in the form of the Fokker-Planck equation. Vetter et al. utilized the Cooper-Chang algorithm to numerically solve the ordinary differential equation [27]. The Cooper-Chang algorithm provides a practical finite difference scheme for the initial value problems of the Fokker-Planck equation while satisfying the intrinsic properties of the equation [39]. The algorithm allows for a variable mesh size, significantly reducing the number of mesh points and the amount of calculations [39].

The Cooper-Chang algorithm begins by obtaining a quasi-equilibrium solution of $\tilde{P}$. Starting from the Fokker-Planck equation, quasi-equilibrium solutions of continuous forms of the number of particles $\tilde{P}$ are obtained from the equation below,

$$\frac{\partial \tilde{P}}{\partial t} = \frac{\partial}{\partial \tilde{n}}\left(A \cdot \tilde{P} + B \cdot \frac{\partial \tilde{P}}{\partial \tilde{n}}\right), \tag{8}$$

where A and B are the drift velocity and the dispersion coefficient, respectively. They can be expressed as

$$A = -v + \frac{1}{2} \cdot \frac{\partial H}{\partial \tilde{n}} \tag{9}$$

$$B = \frac{1}{2} \cdot H \tag{10}$$

In Eq. (8), terms inside the parenthesis represent the total flux j at position ñ and t. Utilizing the total flux term transforms Eq. (8) into the following form.

$$\left.\frac{\partial \tilde{P}}{\partial t}\right|_m = \frac{1}{\Delta \tilde{n}_{m-1,\, m+1}}(j_{m+1/2} - j_{m-1/2}) \tag{11}$$

The unique trait of the Cooper-Chang algorithm is that instead of the centered difference scheme, a variable differencing scheme is adopted to prevent negative values for $\tilde{P}$. Therefore, $\tilde{P}$ and j can be expressed as

$$\tilde{P}_{m+1/2} = (1-\delta_m)\tilde{P}_{m+1} + \delta_m \tilde{P}_m \tag{12}$$

$$\begin{aligned} j_{j+1/2} = &\left((1-\delta_m)A_{m+1/2} + \frac{1}{\Delta \tilde{n}_{m,\, m+1}} B_{m+1/2}\right)\tilde{P}_{m+1} \\ &- \left(\frac{1}{\Delta \tilde{n}_{m,\, m+1}} B_{m+1/2} - \delta_m A_{m+1/2}\right)\tilde{P}_m \end{aligned} \tag{13}$$

where δ_m is a value between 0 and 1/2, which indicates the type of the difference scheme. δ_m having a value of 0 implies the use of the forward difference scheme whereas δ_m having a value of 1/2 implies the use of the centered difference scheme.

As we formulate the value of $\tilde{P}$, the difference between the particle numbers of two adjacent mesh points can be described as below:

$$\frac{\tilde{P}_{m+1}}{\tilde{P}_m} = \frac{\frac{1}{\Delta \tilde{n}_{m,\, m+1}} B_{m+1/2} - \delta_m A_{m+1/2}}{\frac{1}{\Delta \tilde{n}_{m,\, m+1}} B_{m+1/2} + (1-\delta_m) A_{m+1/2}} \tag{14}$$

$$\backsimeq \exp\left[-\int_{\tilde{n}_m}^{\tilde{n}_{m+1}} \frac{A}{B} d\tilde{n}\right] \tag{15}$$

$$\backsimeq \exp\left[-\frac{A_{m+1/2}}{B_{m+1/2}} \Delta \tilde{n}_{m,\, m+1}\right] \tag{16}$$

To simplify Eqs. (14)-(16), a new quantity w is introduced. It can be formulated as

$$w_{m+1/2} = \frac{A_{m+1/2}}{B_{m+1/2}} \Delta \tilde{n}_{m,\, m+1} \tag{17}$$

Combining Eqs. (14), (16), and (17) leads to

$$\exp(-w_{m+1/2}) = \frac{\frac{B_{m+1/2}}{\Delta \tilde{n}_{m,\, m+1}} - A_{m+1/2}\delta_m}{\frac{B_{m+1/2}}{\Delta \tilde{n}_{m,\, m+1}} + A_{m+1/2}(1-\delta_m)} \tag{18}$$

$$= \frac{1 - w_{m+1/2}\delta_m}{1 + w_{m+1/2}(1-\delta_m)} \tag{19}$$

Solving Eq. (19) for δ_m yields

$$\delta_m = \frac{1}{w_{m+1/2}} - \frac{1}{\exp(w_{m+1/2}) - 1}, \tag{20}$$

which is the second objective in the Cooper-Chang algorithm.

Finally, the expression for the intermediate flux $j_{m+1/2}$ is achieved by substituting δ_m in Eq. (13) with Eq. (20).

$$j_{m+1/2} = \frac{B_{m+1/2}}{\Delta \tilde{n}_{m,\, m+1}}[\{w_{m+1/2}(1-\delta_m)+1\}\tilde{Y}_{m+1} - (1 - w_{m+1/2}\delta_m)\tilde{Y}_m] \tag{21}$$

$$= \frac{B_{m+1/2}}{\Delta \tilde{n}_{m,\, m+1}}\left[\frac{w_{m+1/2}}{1-\exp(-w_{m+1/2})}\tilde{Y}_{m+1} - \frac{-w_{m+1/2}}{1-\exp(w_{m+1/2})}\tilde{Y}_m\right] \tag{22}$$

For the sake of further simplification, a new term W is introduced.

$$W^{\pm}_{m+1/2} = \frac{\pm w_{m+1/2}}{1 - \exp(\mp w_{m+1/2})} \tag{23}$$

By substituting Eqs. (22) and (23) into Eq. (8), the final equation in the Cooper-Chang algorithm is obtained.

$$\begin{aligned} \frac{d\tilde{Y}_m}{d\tau} = &\frac{1}{\Delta \tilde{n}_{m-1,\, m+1}}\left[\frac{B_{m+1/2}}{\Delta \tilde{n}_{m,\, m+1}}(W^+_{m+1/2}\tilde{Y}_{m+1} - W^-_{m+1/2}\tilde{Y}_m)\right. \\ &\left. - \frac{B_{m-1/2}}{\Delta \tilde{n}_{m-1,\, m}}(W^+_{m-1/2}\tilde{Y}_m - W^-_{m-1/2}\tilde{Y}_{m-1})\right] \end{aligned} \tag{24}$$

$$= a_m \tilde{Y}_{m-1} - b_m \tilde{Y}_m + c_m \tilde{Y}_{m+1} \tag{25}$$

From Eq. (25), the implicit difference equation can be solved by applying the back-substitution algorithm.

2. Modifications in the Original KRE Model

To extend the original KRE model explained in Vetter et al. to also consider the isothermal condition, the modeling was repeated several hundred times, with each iteration running for only a short duration of time. The temperature changed on a small scale from one iteration of the model to the next, reflecting only a gradual change in temperature. Each run of the model inherited the final crystal distribution from the previous run, setting it to be the new run's initial crystal distribution. Therefore, each model picked up from where the previous model left off, thus, smoothly integrating the entire simulation into a whole, with minimum discrepancy between each simulation of the model. While the temperature difference between consecutive models and the time taken in each run

Table 1. Solubilities of each solution considered in this study

	Solubility
Ammonium sulfate aqueous solution	$1.60\times10^{-4}\times T^2+1.87\times10^{-2}\times T+7.09$ [g/1 L H_2O]
Dodecanol - decanol binary system	$1.88\times10^{-1}\times T+10.47$ [g/1 L Dodecanol]
Potassium chloride aqueous solution	$2.38\times T+284.74$ [g/1 L H_2O]
Ethyl vanillin aqueous solution	$1.22\times10^{-5}\times T^2+1.16\times10^{-4}\times T+7.92\times10^{-3}$ [g/1 L H_2O]

differ from one simulation to another, the temperature difference and time taken in each model do not exceed 0.1 °C and 1 second, respectively, to secure sufficient smoothness between the consecutive models.

Next, the temperature-dependency of each variable should be considered. Solubility is the most important variable in the cooling crystallization process, and the solubility should be expressed as a function of solution temperature. The solubility functions used in the following sections of this study are summarized in Table 1.

Finally, some of the equations in the original KRE model should be modified to describe the crystallization behavior in cooling crystallization. In the original KRE model by Vetter et al., it is known that the critical radius of a crystallization system depends on the degree of supersaturation.

$$\text{Critical Radius} = \left[\frac{\alpha}{\ln(S)}\right]^3 \tag{26}$$

where α is capillary length of the crystal and S is the degree of supersaturation expressed as below [27].

$$S = \frac{c^*}{c} \tag{27}$$

where c^* is the concentration of solute at each condition and c is the bulk solubility.

In this modified simulation considering cooling crystallization, the degree of supersaturation is not only changed by the inflow and outflow of particles by growth and dissolution, but also by the change in temperature. Under a cooling crystallization system, the degree of supersaturation increases as the crystallization temperature decreases. The increased supersaturation reduces the critical radius until it reaches the particle cluster distribution size inside the suspended liquid. This behavior has been graphically described in Fig. 2.

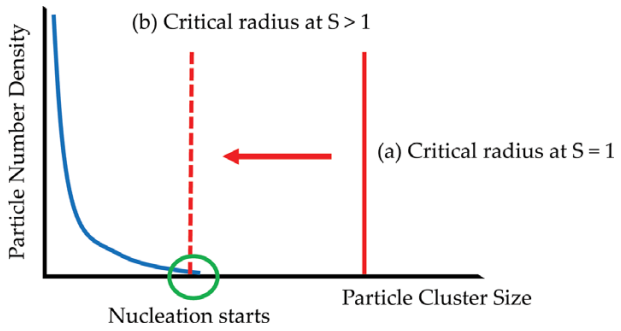

Fig. 2. Movement of critical radius due to supersaturation. Solid line (a) indicates the size of critical radius at S=1, while the dotted line (b) indicates the decreased size of critical radius at S>1.

At the saturated solubility of the solution (S=1), the critical size is located at the solid line (a) in Fig. 2. Solubility is usually dependent on each particle size [40], so the bulk solubility and the solubility of small-sized particles are different. Because the critical radius is larger than the particle cluster size in the suspended liquid, the solubility of small-sized particle clusters is treated as undersaturated, while the bulk solubility is regarded as supersaturated. Therefore, no nucleation occurs in this situation. When the solution temperature is decreased by cooling to increase the degree of supersaturation, the critical radius is also decreased as described in Eq. (26). When the critical radius reaches the location noted by the dotted line (b) in Fig. 2, it will be smaller than some of the particle clusters inside the suspended liquid. From that point on, the particle clusters larger than the critical radius will start to grow as monomers are attached to them, because these particle clusters are treated as supersaturated. Using this mechanism, nucleation and the metastable zone width can be simulated by the KRE model.

However, the original KRE model by Vetter et al. may require an excessive degree of supersaturation to describe nucleation. Unseeded simulations did not show any sign of nucleation up to the degree of supersaturation of 2.25 [27]. While the simulations proved that the original KRE model can describe nucleation at an unseeded solution with varying degrees of supersaturation, the resulting induction time was not compatible with those of experiments from previous literature at this high degree of supersaturation [41,42].

Therefore, the growth rate and effective dispersion rate had to be modified. Newly added variable v and H in Eq. (7) are the growth rate and effective dispersion rate, respectively, given by

$$v(\tilde{n}) = g_{\tilde{n}} \cdot P_1 - h_{\tilde{n}} \tag{28}$$

$$H(\tilde{n}) = g_{\tilde{n}} \cdot P_1 + h_{\tilde{n}} \tag{29}$$

Substituting Eq. (2) and (3) to (28) and (29) results in

$$v(\tilde{n}) = k \cdot \tilde{n}^a \cdot P_1 - k \cdot \tilde{n}^a \cdot P_{1,\infty} \cdot \exp\left(\frac{\alpha}{\tilde{n}^{1/3}}\right) \tag{30}$$

$$H(\tilde{n}) = k \cdot \tilde{n}^a \cdot P_1 + k \cdot \tilde{n}^a \cdot P_{1,\infty} \cdot \exp\left(\frac{\alpha}{\tilde{n}^{1/3}}\right) \tag{31}$$

In the original KRE model, nucleation occurs as the varying critical radius decreases until it reaches the size of largest particle inside the suspended liquid. Therefore, the lack of nucleation indicates that the originally allocated value of growth and dispersion rate had to be modified to fit the resulting induction time into the experimental data.

Thus, the equation for the estimation of critical radius was modified, which in turn was reflected in the kinetic parameter on the detachment rate parameter, h_n. Eq. (3) is therefore modified by the following equation.

$$h_n = k^* \cdot n^a \cdot Y_1^*(n) \quad (32)$$

$$\text{for } k^* = \alpha \cdot k \quad (33)$$

While the empirical value α varies due to properties of solute, it is set between 1/2 and 1/3.

Finally, as Eq. (33) is substituted into Eq. (30) and Eq. (31), Eq. (30) and Eq. (31) become

$$v(\tilde{n}) = k \cdot \tilde{n}^a \cdot P_1 - k^* \cdot \tilde{n}^a \cdot P_{1,\infty} \cdot \exp\left(\frac{\alpha}{\tilde{n}^{1/3}}\right) \quad (34)$$

$$H(\tilde{n}) = k \cdot \tilde{n}^a \cdot P_1 + k^* \cdot \tilde{n}^a \cdot P_{1,\infty} \cdot \exp\left(\frac{\alpha}{\tilde{n}^{1/3}}\right) \quad (35)$$

RESULTS AND DISCUSSION

1. Validation of the Modified KRE Model

In this section, the crystal growth of ammonium sulfate was examined to validate the modified KRE model that was developed. Experimental data of a similar crystal growth work from Hu et al. was utilized for the validation [43]. The initial seed distribution had a mean size of 255 μm as shown in Fig. 3(b). The temperature was decreased in accordance with the cooling profile in Fig. 3(a). The cooling profile is the same as that in the experiment (experiment #2) detailed in the previous work by Hu et al. [43]. The change in solubility with temperature was reflected using Eq. (27). The molecular weight and crystal density of ammonium sulfate were fixed as 132.14 g/mol and 1,770 kg/m^3, respectively.

From Fig. 3(b), it can be seen that the seed supplied at a mean size of 255 μm grew to 713 μm, which is reasonably similar to the experimental results from previous literature (from 255 μm to 700 μm) [43]. In the previous literature, the population balance equation was employed to follow up the crystal growth of seeded crystallization [43]. From the results in this study, the crystal growth movement of the actual experimental data can be simulated by the modified KRE model successfully. Further, the performance of the modified KRE model for simulating crystal growth is comparable with the performance of the conventional population balance model.

2. Metastable Zone width Estimation

The metastable zone width is defined as the maximum degree of supersaturation where crystal growth can be measured during which time no nucleation can be found at a constant cooling condition. The metastable zone width should be artificially incorporated into the population balance equation model by modifying the growth and nucleation rate equations [44-46]. However, the modified KRE model can simulate the metastable zone width without any modification in the model. To investigate the applicability of the model for the estimation of metastable zone width, a comparative analysis between the experimental data of the dodecanol-decanol crystallization system by Kim and Mersmann and the simulation results from the modified KRE model was conducted [47]. The results are shown in Table 2.

In the modified KRE model, the metastable zone width was determined at the degree of supersaturation where the critical radius became smaller than the size of particle clusters inside the suspended liquid. Nucleation commences at the end of the metastable zone, because the particle clusters larger than the critical radius would begin to grow. Therefore, the maximum subcooling can be calculated from the metastable zone width.

As can be seen in Table 2, the simulation results using the modified KRE model match well with the experimental metastable zone

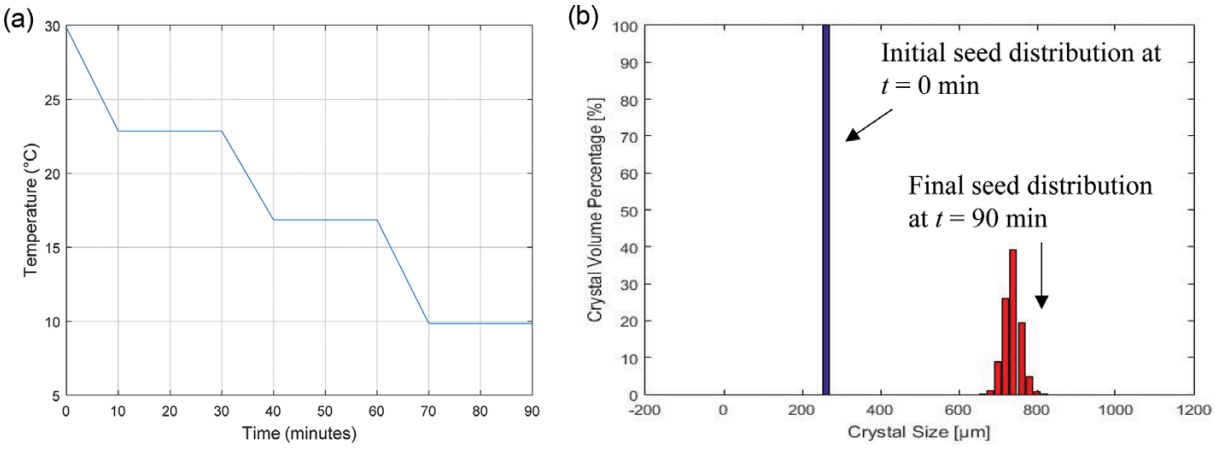

Fig. 3. Crystal growth simulation with a seeded crystallization. (a) Temperature cooling profile, and (b) crystal size distribution at initial and final operation time. In (b), the blue bar graph indicates the initial seed distribution and the red bar graph represents the final crystal distribution.

Table 2. Metastable zone width measurement in previous study [47] and estimation by the modified KRE model at same condition

Saturation temperature [°C]	Cooling rate [°C/min]	Maximum subcooling ΔT [°C] (experimental results)	Maximum subcooling ΔT [°C] (simulation results by modified KRE model)
23	1	1.7	1.5
23	0.1	1.3	1.3

width. As the cooling rate is decreased, the maximum subcooling temperature difference is also decreased. This trend is matched by the experimental observations, and it agrees with the generally accepted characteristic about the metastable zone. Therefore, it can be concluded that the modified KRE model can be applied for simulation of the crystallization system with the metastable zone.

3. Effect of Pre-history in Temperature Profile

In this section, the effect of pre-history in the temperature profile on the crystallization system was investigated. Because many previous studies have demonstrated that the pre-history in the temperature profile during cooling crystallization influences the particle size distribution, induction time, and metastable zone width, the effect of pre-history in the temperature profile should be considered in the crystallization model [35,36,48,49]. However, the conventional population balance equation cannot describe the behavior of sub-nuclei, hence it cannot consider the effect of pre-history in the temperature profile. Therefore, by clarifying the applicability of the modified KRE model in estimating the effect of pre-history in the temperature profile, it can be proven that the modified KRE model is superior in describing the crystallization behavior more precisely. Two cases (potassium chloride and ethyl vanillin) were selected for comparison between the experimental data and the simulation results from the modified KRE model.

3-1. Potassium Chloride

According to the work by Sugimoto et al., the metastable zone width is influenced depending on the pre-history of overheating before the crystallization begins [36]. This behavior can be expressed by the modified KRE model.

At higher temperatures, the Gibbs free energy of the particles increases, thus preferring the formation of smaller particle clusters over larger particle clusters. Therefore, with an overheating condition before crystallization, the particle cluster distribution would be shifted to smaller particle clusters while having a smaller number of larger particle clusters.

In the modified KRE model, nucleation begins when the decreasing critical radius meets the particle clusters below a detectable size of the nuclei as described in Fig. 2. With a smaller number of larger particle clusters, the critical radius should be decreased further to induce nucleation, requiring a larger degree of supersaturation as described in Eq. (26). Therefore, the main hypothesis of this simulation is that the overheating condition before crystallization would result in a shift towards a smaller size of particle cluster distribution inside the suspended liquid, and thus, would create a wider metastable zone width.

To confirm the hypothesis, overheating simulation was conducted and compared with the initial condition. The subject concentration for this simulation was 30 °C saturated potassium chloride aqueous solution. As the initial condition, it was assumed that the particle size distribution of the solution in sub-nuclei size follows the Gaussian distribution with a mean size of 5×10^{-4} μm. Next, the solution was heated to 60 °C from 30 °C. The difference in number density of the particle clusters caused by heating the solution can be calculated by subtracting the number density at 60 °C from that at 30 °C. The results are shown in Fig. 4.

In Fig. 4, it is clearly revealed that the heated solution contained more of smaller-sized particle clusters, while there was a decrease

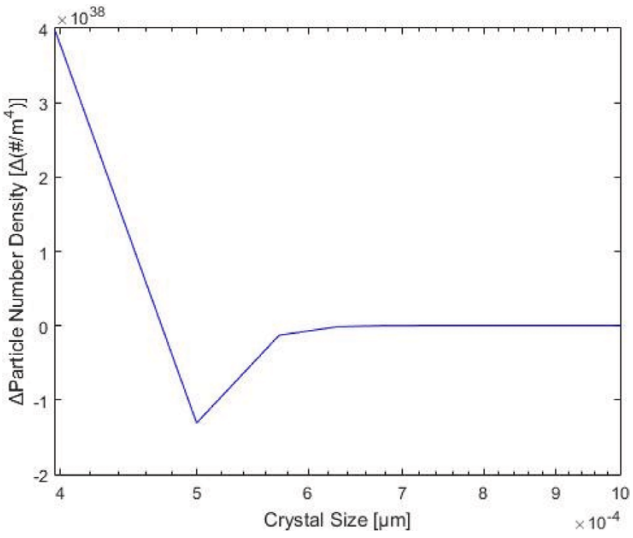

Fig. 4. The difference in number density of particle clusters between the heated solution (60 °C) and the unheated solution (30 °C).

in the number of larger-sized particle clusters. Thus, the hypothesis above was well matched with the simulation results. Note that the particle cluster behavior observed in this simulation is in the region of sub-nuclei size. Because the population balance equation cannot describe these sub-nuclei clusters, this behavior can only be expressed by the modified KRE model.

Next, we examined how accurately the modified KRE model can simulate the actual metastable zone width. Three different cases of 60 °C, 50 °C, and 40 °C saturated potassium chloride aqueous solution were selected. Initially, all cases were heated to above 30 °C from its saturated temperature. Next, the solution temperature was returned to its saturated temperature. After reaching steady-state, cooling crystallization simulation was conducted in each case. The cooling rate was set as 7 °C per minute, as experimented by Sugimoto et al. [36]. In this simulation, the nucleation was defined as a point where a particle cluster larger than 1 μm appeared. In such a case, the metastable zone width can be defined as the temperature difference between the initial temperature and final temperature where nuclei larger than 1 μm would appear. The simulate results and experimental data by Sugimoto et al. are displayed in Fig. 5.

Fig. 5 shows the difference in the metastable zone width between heated and unheated solutions obtained both experimentally and via simulation with the modified KRE model. The simulation results from the modified KRE model can successfully describe the phenomenon wherein the metastable region width increases when the solution was overheated prior to cooling. This validates the hypothesis that a pre-history of overheating induces a larger metastable zone width by shifting the particle cluster distribution towards a smaller size.

3-2. Ethyl Vanillin

Ethyl vanillin was reported to have a larger metastable zone width due to an increased extent of overheating prior to cooling [34]. In this section, we investigated the extent to which overheated temperatures influenced the metastable zone width of ethyl vanillin aqueous solution by using the modified KRE model.

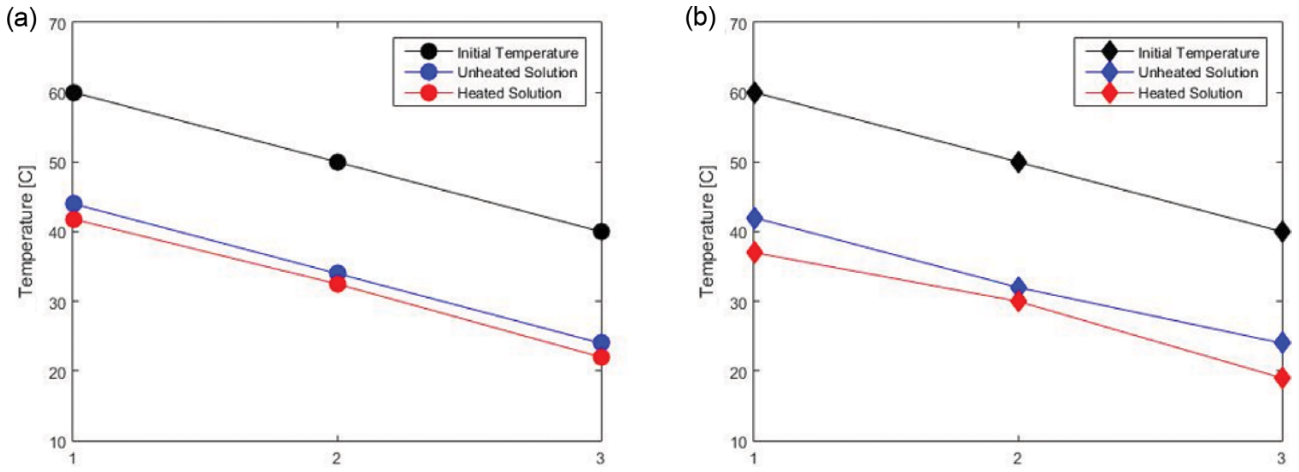

Fig. 5. Difference in metastable zone width between heated and unheated solutions. (a) the difference in the metastable region among the simulation works, and (b) the difference in metastable region among experimental works by Sugimoto et al. [36]. Three cases (initial temperature=60 °C, 50 °C, and 40 °C) were simulated with same cooling rate, and numbered as 1,2,3 on x-axis in this figure, respectively.

To replicate the work by Hussain et al., three simulations regarding ethyl vanillin aqueous solution were prepared. From the saturated solution with an initial temperature of 30 °C, the solutions were (1) immediately cooled, (2) heated to 40 °C and cooled, and (3) heated to 60 °C and cooled, respectively. The cooling rate of the system in all three simulations was set as 3 °C per hour, as indicated in the previous study [34]. If nuclei (larger than 1 μm of particle cluster) in the ethyl vanillin aqueous solution appeared, the simulation was stopped, and the metastable zone width was checked in each simulation condition.

Experimental and simulation results by changing the overheated temperature are shown in Fig. 6. The simulation results are well matched with the experimental data. As the overheated temperature increases, the metastable zone width is enlarged. The modified KRE model can successfully describe the experimental data of the metastable zone width. As well as the metastable zone width simulation caused by pre-heating, the modified KRE model can simulate the change in metastable zone width due to changing overheating temperature. Considering that this type of applicability of the model cannot be found in the population balance equation model, the competitiveness of the modified KRE model was clearly clarified.

To analyze the actual reason for the enlarged metastable zone width in the modified KRE model, the difference of particle number density was compared as in the Section 3.3.1. Fig. 7 shows the difference in the particle cluster number density between the heated and unheated solutions before cooling begins. As hypothesized in Section 3.3.1, the number of smaller particle clusters increased, while the number of larger particles decreased due to overheating. This indicates that the critical radius must decrease further to reach the particle cluster size distribution, requiring a larger degree of supersaturation. Therefore, the metastable zone width would be enlarged to reach the required degree of supersaturation for nucleation. In addition, by increasing the pre-heated temperature as shown in Fig. 6(b), the particle size distribution was shifted towards a smaller size. In that case, the metastable zone width is increased further.

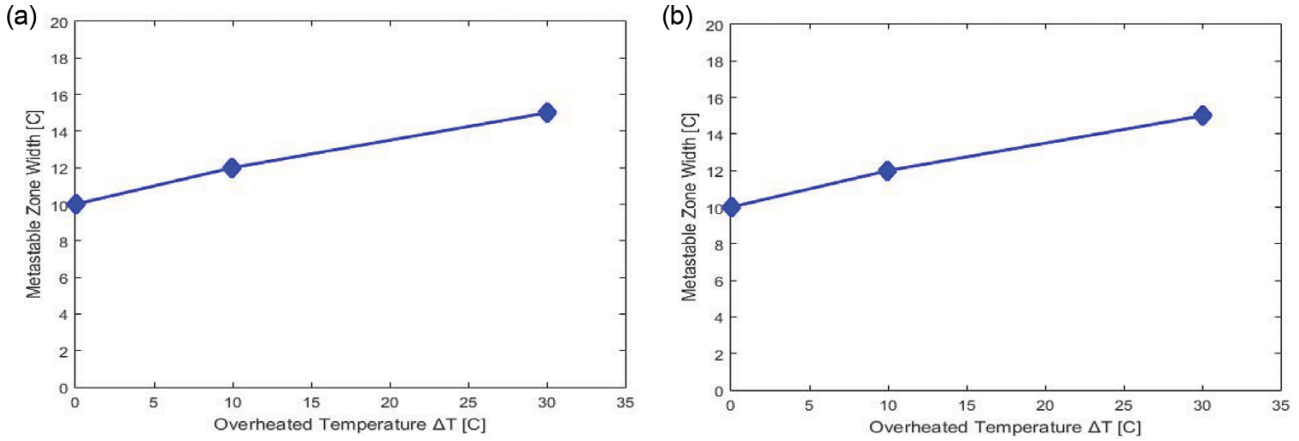

Fig. 6. Metastable zone width of ethyl vanillin aqueous solution by changing overheated temperature. (a) experimental data from Hussain et al. [34], and (b) simulation data from the modified KRE model.

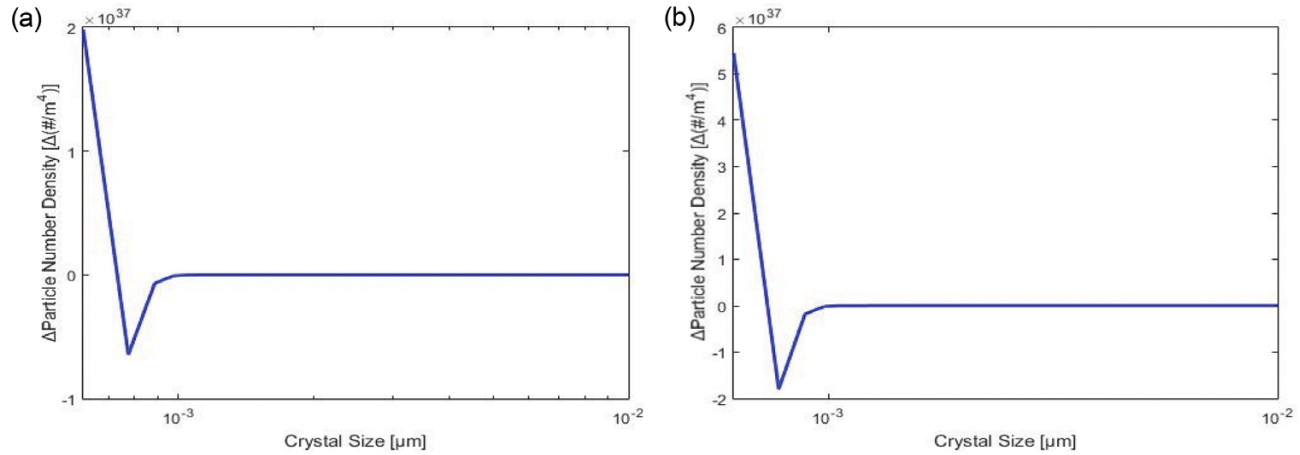

Fig. 7. The difference in number density of particle clusters in ethyl vanillin solution. The difference in number density of particle clusters inside the suspended liquid (a) heated to 40 °C, and (b) heated to 60 °C.

From the analysis results, the main reason for the change in the metastable zone width is clearly identified as the increased overheated temperature in the modified KRE model. This result further validates our hypothesis by discovering the connection between the change in particle cluster distribution size and metastable region width.

CONCLUSIONS

We developed a novel modified KRE model to apply to cooling crystallization by expanding its original assumption of isothermal condition, enabling the KRE model to investigate the crystal growth and metastable region width in cooling crystallization. Therefore, the modified KRE model can extend its applicability to include cooling crystallization, thus overcoming the limitation of the original KRE model.

The performance of the modified KRE model was compared with experimental data from the previous literature. The crystal size growth and the metastable region width through the modified KRE model was validated by comparison with the experimental data from previous literature.

Investigation on the effect of pre-heating before cooling revealed two facts. First, the particle cluster distributions were shifted towards the smaller size when the solutions were heated prior to cooling regardless of the initial temperature, leading to the extended metastable region width. The result validates the main assumption of the modified KRE model that the critical radius varies and nucleation begins when the decreasing critical radius reaches the particle cluster distribution size inside the suspended liquid. Second, the higher the heated temperature, the smaller the particle size distribution seen in the solution. In turn, smaller particle cluster distributions result in greater increments of the metastable region width. These results point out that the shift in the particle cluster distribution inside the solution before cooling may be the result of the extended metastable region width. Because this simulation capability cannot be obtained in the population balance equation model, the results in this study clearly indicate that the modified KRE model has wider applicability in the modeling of crystallization.

Overall, the modified KRE model has certain advantages that lend it a competitive edge in describing crystallization behavior in various situations. Our study has clarified that the original KRE model can be extended to apply to various crystallization systems by modifying the basic structure and assumptions in the original KRE model. The modified KRE model can be applied to model cooling crystallization that is unlike the original KRE model. It is also used in describing the metastable zone width behavior that is unlike the behavior in the population balance equation model. Therefore, the modified KRE model has the potential to be employed in the description of various crystallization processes such as those seen in antisolvents, evaporation, and melt crystallization.

REFERENCES

1. J. W. Mullin, *Crystallization*, Elsevier (2001).
2. M. Fujiwara, Z. K. Nagy, J. W. Chew and R. D. Braatz, *J. Process Control*, **15**, 493 (2005).
3. N. Sanzida and Z. K. Nagy, *Comput. Chem. Eng.*, **130**, 106559 (2019).
4. C. F. C. Marcellos, H. Durand, J. S. I. Kwon, A. G. Barreto, P. L. da Cunha Lage, M. B. de Souza, A. R. Secchi and P. D. Christofides, *AIChE J.*, **64**, 1618 (2018).
5. M. A. McDonald, A. S. Bommarius, R. W. Rousseau and M. A. Grover, *Comput. Chem. Eng.*, **123**, 331 (2019).
6. H. Kim, K. Park, J. W. Chang, T. Lee, S. H. Kim and D. R. Yang, *Cryst. Growth Des.*, **19**, 1748 (2019).
7. K. Park, D. Y. Kim and D. R. Yang, *Ind. Eng. Chem. Res.*, **55**, 7142 (2016).
8. I. H. Leubner, *Curr. Opin. Colloid Interface Sci.*, **5**, 151 (2000).
9. T. Y. Chiu and P. D. Christofides, *AIChE J.*, **46**, 266 (2000).
10. J. S.-I. Kwon, M. Nayhouse, P. D. Christofides and G. Orkoulas, *Chem. Eng. Sci.*, **107**, 47 (2014).
11. J. S.-I. Kwon, M. Nayhouse, G. Orkoulas and P. D. Christofides, *Chem. Eng. Sci.*, **119**, 30 (2014).
12. D. J. Griffin, M. A. Grover, Y. Kawajiri and R. W. Rousseau, *Ind. Eng. Chem. Res.*, **55**, 1361 (2016).
13. H. Li, Y. Kawajiri, M. A. Grover and R. W. Rousseau, *Ind. Eng.*

Chem. Res., **56**, 4060 (2017).
14. D. J. Griffin, Y. Kawajiri, M. A. Grover and R. W. Rousseau, *Cryst. Growth Des.*, **15**, 305 (2014).
15. D. J. Griffin, Y. Kawajiri, R. W. Rousseau and M. A. Grover, *Chem. Eng. Sci.*, **164**, 344 (2017).
16. J. Li, C. J. Tilbury, M. N. Joswiak, B. Peters and M. F. Doherty, *Cryst. Growth Des.*, **16**, 3313 (2016).
17. D. Ramkrishna and M. R. Singh, *Annu. Rev. Chem. Biomol. Eng.*, **5**, 123 (2014).
18. F. Puel, G. Févotte and J. Klein, *Chem. Eng. Sci.*, **58**, 3715 (2003).
19. C. B. B. Costa, M. R. W. Maciel and R. Maciel Filho, *Comput. Chem. Eng.*, **31**, 206 (2007).
20. L. F. Farias, J. A. de Souza, R. D. Braatz and C. A. da Rosa, *Comput. Chem. Eng.*, **123**, 246 (2019).
21. D. Fysikopoulos, B. Benyahia, A. Borsos, Z. K. Nagy and C. D. Rielly, *Comput. Chem. Eng.*, **122**, 275 (2019).
22. B. Szilágyi, P. S. e. Agachi and Z. n. K. Nagy, *Ind. Eng. Chem. Res.*, **57**, 3320 (2018).
23. S. Sulttan and S. Rohani, *J. Cryst. Growth*, **505**, 19 (2019).
24. C. A. da Rosa and R. D. Braatz, *Ind. Eng. Chem. Res.*, **57**, 11702 (2018).
25. H. M. Hulburt and S. Katz, *Chem. Eng. Sci.*, **19**, 555 (1964).
26. A. Randolph and M. Larson, Theory of particulate technology, Academic Press, New York (1971).
27. T. Vetter, M. Iggland, D. R. Ochsenbein, F. S. Hänseler and M. Mazzotti, *Cryst. Growth Des.*, **13**, 4890 (2013).
28. X. Fu, D. Zhang, S. Xu, B. Yu, K. Zhang, S. Rohani and J. Gong, *Cryst. Growth Des.*, **18**, 2851 (2018).
29. F. Anisi and H. J. Kramer, *Chem. Eng. Res. Des.*, **138**, 200 (2018).
30. D. Kashchiev, *Nucleation*, Elsevier (2000).
31. L. Farkas, *Z. Phys. Chemie.*, **125**, 236 (1927).
32. I. Stranski and R. Kaischew, *Ann. Phys.*, **415**, 330 (1935).
33. R. Becker and W. Döring, *Ann. Phys.*, **416**, 719 (1935).
34. K. Hussain, G. Thorsen and D. Malthe-Sørenssen, *Chem. Eng. Sci.*, **56**, 2295 (2001).
35. F. L. Nordström, M. Svärd, B. Malmberg and Å. C. Rasmuson, *Cryst. Growth Des.*, **12**, 4340 (2012).
36. T. Sugimoto, A. Mori and T. Inoue, *J. Cryst. Growth*, **292**, 108 (2006).
37. I. Lignos, R. Maceiczyk and A. J. deMello, *Acc. Chem. Res.*, **50**, 1248 (2017).
38. Y. Tahri, Z. Kozisek, E. Gagnière, E. Chabanon, T. Bounahmidi and D. Mangin, *Cryst. Growth Des.*, **16**, 5689 (2016).
39. J. Chang and G. Cooper, *J. Comput. Phys.*, **6**, 1 (1970).
40. M. Iggland and M. Mazzotti, *Cryst. Growth Des.*, **12**, 1489 (2012).
41. M. Trifkovic, M. Sheikhzadeh and S. Rohani, *J. Cryst. Growth*, **311**, 3640 (2009).
42. M. Lenka and D. Sarkar, *J. Cryst. Growth*, **408**, 85 (2014).
43. Q. Hu, S. Rohani, D. Wang and A. Jutan, *AIChE J.*, **50**, 1786 (2004).
44. D. R. Yang, K. S. Lee, J. S. Lee, S. G. Kim, D. H. Kim and Y. K. Bang, *Ind. Eng. Chem. Res.*, **46**, 8158 (2007).
45. S. S. Kadam, S. A. Kulkarni, R. C. Ribera, A. I. Stankiewicz, J. H. ter Horst and H. J. Kramer, *Chem. Eng. Sci.*, **72**, 10 (2012).
46. M. Kobari, N. Kubota and I. Hirasawa, *CrystEngComm*, **15**, 1199 (2013).
47. K.-J. Kim and A. Mersmann, *Chem. Eng. Sci.*, **56**, 2315 (2001).
48. J. Ulrich and C. Strege, *J. Cryst. Growth*, **237**, 2130 (2002).
49. S. Qi, P. Avalle, R. Saklatvala and D. Q. Craig, *Eur. J. Pharm. Biopharm.*, **69**, 364 (2008).